Graphene with Rashba spin-orbit interaction and coupling to a magnetic layer: Electron states localized at the domain wall

M. Inglot,[1] V. K. Dugaev,[1] A. Dyrdał,[2] and J. Barnaś[2,3]

[1]*Department of Physics and Medical Engineering, Rzeszów University of Technology, al. Powstańców Warszawy 6, 35-959 Rzeszów, Poland*

[2]*Faculty of Physics, Adam Mickiewicz University, ul. Uniwersytetu Poznańskiego 2, 61-614 Poznań, Poland*

[3]*Institute of Molecular Physics, Polish Academy of Sciences, ul. M. Smoluchowskiego 17, 60-179 Poznań, Poland*

(Received 11 July 2020; accepted 22 November 2021; published 6 December 2021)

Electron states localized at a magnetic domain wall in a graphene with Rashba spin-orbit interaction and coupled to a magnetic layer are studied theoretically. It is shown that two one-dimensional bands of edge modes propagating along the domain wall emerge in the energy gap for each Dirac point, and the modes associated with different Dirac points K and K' are the same. The coefficients describing decay of the corresponding wave functions with distance from the domain wall contain generally real and imaginary terms. Numerical results on the local spin density and on the total spin expected in the edge states characterized by the wave number k_y are presented and discussed. The Chern number for a single magnetic domain on graphene indicates that the system is in the quantum anomalous Hall phase, with two chiral modes at the edges. In turn, the number of modes localized at the domain wall is determined by the difference in Chern numbers on both sides of the wall. These numbers are equal to 2 and -2, respectively, so there are four modes localized at the domain wall.

DOI: 10.1103/PhysRevB.104.214408

I. INTRODUCTION

It is well known that a two-dimensional electron gas appears at the interface of two different insulators with nonequivalent topology of electron bands [1,2]. A typical example is the interface between an ordinary insulator (or vacuum) and a three-dimensional topological insulator (for instance, Bi_2Te_3) [3] or a crystalline topological insulator [4,5]. The low-energy spectrum of electron states at the interface can be then described by the massless relativistic Dirac Hamiltonian.

A characteristic feature of the topological nonequivalence of two materials in contact is the inversion of energy bands at the interface. An interesting example is the two-dimensional Dirac electron gas with perpendicular magnetization that induces the energy gap Δ in the Dirac spectrum [6–8]. This spectrum does not depend on the sign of Δ; however, the energy bands become inverted at the interface between regions with $\Delta > 0$ and $\Delta < 0$. As a result, an additional one-dimensional energy band of electron states localized at the boundary separating the areas of $\Delta > 0$ and $\Delta < 0$ appears in the system. This can be also considered as the appearance of electron states coupled to the magnetic domain wall. Interestingly, such electron states in topological insulators with a magnetic layer on top are responsible for nondissipative equilibrium currents along the domain wall [9–11].

It should be noted that the basic idea of electron states bound to the kink of a static scalar field was formulated long ago by Jackiw and Rebbi [12], who demonstrated the existence of zero-energy electron states in the systems of Dirac and Yang-Mills fermions. Using various realizations of this idea one can find zero-energy solutions at the contact of narrow-gap semiconductors with mutually inverted energy bands [13], at the vortices in chiral superconductors [14], at hedgehogs in superconductors with coexisting singlet and triplet pairing [15], and in the spectrum of surface electrons with a gap inversion in topological insulators [16].

It has been shown recently that the spin-orbit interaction can play an important role when considering the edge states, leading, e.g., to spin polarization of the boundary. An example is a sharp p-n junction in graphene in the presence of spin-orbit coupling and magnetic field [17]. In such a case electron zero modes with linear dispersion appear at the p-n junction, and the corresponding electron states are spin polarized. In one-dimensional models with Rashba spin-orbit coupling (Rashba nanowires) and external magnetic field, some unusual properties (e.g., equilibrium spin currents and localized spin torque) can appear, which are related to emerging edge states at the boundaries between magnetic [18] or Rashba-coupling [19,20] domain walls.

In this paper we consider a graphene-based structure consisting of a graphene monolayer deposited on a substrate that ensures the Rashba spin-orbit interaction [21,22] and covered by a magnetic layer with a domain wall, as presented in Fig. 1(a). The magnetic and spin-orbital proximity effects induced in graphene are important ingredients of the model, since both of them modify the energy spectrum substantially. The magnetization of the capping layer is assumed to be perpendicular to the graphene plane (i.e., it is along the axis z in Fig. 1) and coupled to the graphene either by exchange or stray fields. A uniform proximity-induced magnetization in graphene (no spin-orbit coupling) shifts the spin up/down bands upward/downward, respectively, but leaves the two zero-energy crossing points in the vicinity of the K and K'

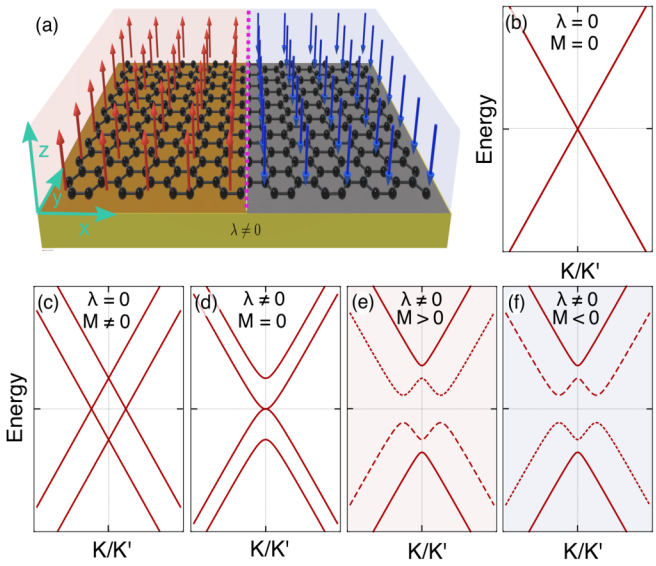

FIG. 1. (a) Schematic picture of the structure: single layer of graphene sandwiched between a substrate inducing Rashba spin-orbit coupling and a magnetic layer with a domain wall. (b)–(f) Schematic band structure of graphene in the absence of magnetization and Rashba coupling (b); in the presence of magnetization, $M \neq 0$ (c); in the presence of Rashba coupling, $\lambda \neq 0$ (d); and in the presence of both magnetization and Rashba coupling (e),(f). Though the band structure for $M > 0$ and $M < 0$ is the same, the bands on the two sides are inverted.

points [see Figs. 1(b) and 1(c)]. In turn, the Rashba spin-orbit interaction induces spin mixing and lifts the fourfold degeneracy at the K/K' points, as presented in Fig. 1(d) [23]. When both proximity-induced magnetization and Rashba spin-orbit interaction are present in the system, the bulk energy gap is opened and all four bands around the Dirac points are nondegenerate [see Figs. 1(e) and 1(f)]. Thus, both magnetic and spin-orbit proximity effects enable controlling the electronic structure and also electric and magnetic properties of the graphene-based systems under consideration. Importantly, when Rashba spin-orbit interaction and magnetization (Zeeman-like field) are simultaneously present in graphene, one can observe the quantum anomalous Hall effect phase with quantized value of the Hall conductance when the Fermi level is inside the energy gap.

We show that creating a domain wall in the magnetic layer leads to further possibilities of controlling electronic and transport properties [24–26]. In particular, we show that the domain wall generates conductive states inside the bulk energy gap. These states are localized at the domain wall and lead to additional functionality of the graphene-based structure because the magnetic domain wall can be controlled by current and/or magnetic field [27–30].

It is worth noting that the influence of domain walls on the electronic spectrum in graphene has been already discussed in the literature. However, the domain walls were of different origin and were related to the possible stacking faults in bilayer [22] or multilayer [31] graphene. Another type of domain walls in gapped graphene, which can appear due to a substrate (like hexagonal boron nitride) with a linear symmetry-breaking defect, was considered by Semenoff *et al.* [32]. They demonstrated the existence of localized states at the domain walls, and pointed out their importance for possible applications.

Using the effective model describing low-energy excitations in a magnetized graphene with Rashba spin-orbit interaction, we calculate the energy and wave functions of the edge states localized at the magnetic domain wall. These modes exist in the gap and propagate along the domain wall. Furthermore, the modes with opposite wave vectors (with respect to K/K' points) have different energy, $\varepsilon(k_y) \neq \varepsilon(-k_y)$. We show that two edge modes (referred to also as chiral modes) appear in the spectrum for each Dirac point, and the modes associated with different Dirac points K and K' are the same. We also show that the attenuation factors that describe decay of the wave functions of chiral modes with distance from the domain wall contain imaginary terms. Accordingly, the corresponding local values of expected physical quantities include an oscillatory contribution with the amplitude decaying with the distance from the wall. As an example, we present numerical results on the local spin density and total spin expected in the edge states.

In Sec. II we describe the model studied in this paper. Electronic states localized at the domain wall are calculated in Sec. III for $k_y = 0$, and in Sec. IV for the case of nonzero k_y. In Sec. IV we also present dispersion curves of the modes propagating along the wall for both K and K' Dirac points. Numerical results on the local spin density in the edge states are presented and discussed in Sec. V. Topological aspects are studied in Sec. VI, whereas the summary and final conclusions are in Sec. VII. Symmetry relations of the model and scattering processes are discussed in Appendices A and B, respectively.

II. MODEL OF GRAPHENE WITH A MAGNETIC DOMAIN WALL

We consider a graphene monolayer deposited on a substrate which generates Rashba spin-orbit interaction [33–37]. In addition, we assume a thin magnetic layer on top of the graphene [38] with magnetization perpendicular to the graphene plane. Coupling to the magnetization opens then a gap in the electronic spectrum of graphene. In this paper we consider a more general situation, when the magnetization is not uniform but forms two domains separated by a narrow domain wall as shown schematically in Fig. 1(a).

Effective Hamiltonian describing low-energy electronic states near the K point of the Brillouin zone in the system under consideration can be written in the form [39]

$$\hat{H}_K = -iv\,(\tau_x\partial_x + \tau_y\partial_y) + \lambda(\sigma_y\tau_x - \sigma_x\tau_y) + \sigma_z M(x), \quad (1)$$

where $v = \hbar v_F \simeq \hbar c/300$, $\boldsymbol{\tau}$ and $\boldsymbol{\sigma}$ represent the vectors of Pauli matrices in the sublattice and spin spaces, respectively, λ is the Rashba spin-orbit coupling parameter, and $M(x)$ is the x-dependent gap parameter that is related to the magnetization in the z direction (perpendicular to the graphene plane). We assume $M(x)$ in the following form [32]:

$$M(x) = \begin{cases} M_0, & x < 0 \\ -M_0, & x \geqslant 0, \end{cases} \quad (2)$$

which describes a sharp magnetic domain wall located at $x = 0$ and uniform along the y axis, as shown schematically in Fig. 1(a). We note that such very sharp domain walls can be created artificially in real systems [40]. The bulk (two-dimensional) electronic band structure of graphene corresponding to $M > 0$ is the same as that for $M < 0$, as presented in Figs. 1(e) and 1(f), respectively. However, the bands become inverted when M changes sign at the domain wall, which is also indicated in Figs. 1(e) and 1(f).

The energy gap in the electronic spectrum of a uniformly magnetized graphene (no domain wall) with Rashba spin-orbit interaction is given by the following formula [41]:

$$E_g = \frac{2|M_0\lambda|}{\sqrt{M_0^2 + \lambda^2}}. \tag{3}$$

This gap is determined by the absolute value of the magnetization, $|M| = M_0$, and the absolute value of the Rashba parameter, $|\lambda|$. Note, the gap vanishes when either $M_0 = 0$ or $\lambda = 0$.

Due to the band inversion, electronic states localized at the domain wall emerge in the energy gap. Using the Schrödinger equation, $(\hat{H} - \varepsilon)\,\psi(\mathbf{r}) = 0$, and taking into account structure geometry, one can write the wave function in the form $\psi(\mathbf{r}) = e^{ik_y y}\,\psi_{k_y}(x)$, where $\psi_{k_y}(x)$ is a bispinor with four components,

$$\psi_{k_y}^T = (\varphi_{k_y}^{\uparrow}, \varphi_{k_y}^{\downarrow}, \chi_{k_y}^{\uparrow}, \chi_{k_y}^{\downarrow}). \tag{4}$$

In the following we will solve the Schrödinger equation and calculate the energy spectrum of the edge states localized at the domain wall.

III. STATES LOCALIZED AT THE DOMAIN WALL FOR $k_y = 0$

Let us consider first the states localized at the domain wall for $k_y = 0$. Equations for the wave-function components (4) for $x < 0$ and $x > 0$ acquire then the following form:

$$\begin{aligned}
&(M - \varepsilon)\,\varphi_0^{\uparrow} - iv\,\partial_x\chi_0^{\uparrow} = 0,\\
&(M + \varepsilon)\,\varphi_0^{\downarrow} - 2i\lambda\chi_0^{\uparrow} + iv\,\partial_x\varphi_0^{\downarrow} = 0,\\
&iv\,\partial_x\varphi_0^{\uparrow} + 2i\lambda\varphi_0^{\downarrow} - (M - \varepsilon)\,\chi_0^{\uparrow} = 0,\\
&iv\,\partial_x\varphi_0^{\downarrow} + (M + \varepsilon)\,\chi_0^{\downarrow} = 0,
\end{aligned} \tag{5}$$

where $M = M_0$ $(x < 0)$ and $M = -M_0$ $(x > 0)$. For states localized at the domain wall one can write the wave functions $\chi_0^{\uparrow,\downarrow}$ and $\varphi_0^{\uparrow,\downarrow}$ in the form

$$\begin{aligned}
&\varphi_0^{\uparrow}(x) = Ae^{\kappa x}, \qquad \varphi_0^{\downarrow}(x) = Be^{\kappa x},\\
&\chi_0^{\uparrow}(x) = Ce^{\kappa x}, \qquad \chi_0^{\downarrow}(x) = De^{\kappa x},
\end{aligned} \tag{6}$$

where A, B, C, D are certain constants, while κ describes a wave-function decay on both sides of the domain wall. Thus, the real value of κ must be positive, $\mathrm{Re}\,\kappa > 0$, for $x < 0$ and negative, $\mathrm{Re}\,\kappa < 0$, for $x > 0$. Upon substituting Eq. (6) into Eq. (5) one obtains a system of linear algebraic equations for the constants A, B, C, D, which has nonzero solutions if the corresponding determinant vanishes. This leads to the following equation for κ:

$$\begin{aligned}
&v^4\kappa^4 + 2v^2M_0^2\kappa^2 + 2v^2\varepsilon^2\kappa^2 + M_0^4 - 2M_0^2\varepsilon^2\\
&\quad + 4M_0^2\lambda^2 - 4\varepsilon^2\lambda^2 + \varepsilon^4 = 0.
\end{aligned} \tag{7}$$

Note, this equation holds for $x > 0$ and $x < 0$. From this we find four solutions denoted as κ_n $(n = 1, 3)$ and κ_p $(p = 2, 4)$,

$$\kappa_n = \frac{1}{v}\left(-M_0^2 - \varepsilon^2 \pm 2\sqrt{M_0^2\varepsilon^2 - M_0^2\lambda^2 + \varepsilon^2\lambda^2}\right)^{1/2}, \tag{8}$$

$$\kappa_p = -\frac{1}{v}\left(-M_0^2 - \varepsilon^2 \pm 2\sqrt{M_0^2\varepsilon^2 - M_0^2\lambda^2 + \varepsilon^2\lambda^2}\right)^{1/2}. \tag{9}$$

The above solutions for κ are complex in general. However, we find that $\mathrm{Re}\,\kappa_1 = \mathrm{Re}\,\kappa_3 > 0$ (so they correspond to $x < 0$) and $\mathrm{Re}\,\kappa_2 = \mathrm{Re}\,\kappa_4 < 0$ (and correspond to $x > 0$).

Upon determining the coefficients A, B, C, D in Eqs. (6), one can write two possible solutions of the Schrödinger equation for $x < 0$ and $x > 0$ in the following form:

$$\psi_{n(p)}(x) = e^{\kappa_{n(p)}x}\begin{pmatrix} 1 \\ -\frac{-k_y^2v^2+\kappa_{n(p)}^2v^2+(M\pm\varepsilon)^2}{2\lambda v(k_y+\kappa_{n(p)})} \\ \pm\frac{i(M\pm\varepsilon)}{v(k_y+\kappa_{n(p)})} \\ \pm\frac{i(k_y-\kappa_{n(p)})\left(\kappa_{n(p)}^2v^2-k_y^2v^2+(\varepsilon+M)^2\right)}{2\lambda(k_y+\kappa_{n(p)})(M\mp\varepsilon)} \end{pmatrix}, \tag{10}$$

where the index n and the upper sign correspond to $x < 0$, whereas the index p and the lower sign correspond to $x > 0$. Since the real part of κ_n is positive and that of κ_p is negative, one can write a general normalized wave function corresponding to the states localized at the domain wall, i.e., the wave function that exponentially decays with distance from the wall on both sides (for $x < 0$ and $x > 0$) in the form

$$\psi(x) = N[a_1\psi_1(x) + a_3\psi_3(x)], \quad x < 0, \tag{11}$$

$$\psi(x) = N[a_2\psi_2(x) + a_4\psi_4(x)], \quad x > 0, \tag{12}$$

where $a_1, \ldots, a_4$ are certain coefficients, which have to be determined from the continuity condition of the wave function at $x = 0$, and N is a normalization factor. From this condition one obtains a system of four linear algebraic equations for $a_1, \ldots, a_4$ in Eqs. (11) and (11). Vanishing of the corresponding determinant defines the energy of the localized states, which can be formally presented in the simple analytical form

$$\varepsilon_{1,2} = \frac{1}{3}\sqrt{3{M_0}^2 + 4\lambda^2}\left(\sqrt{3}\sin\gamma_{1,2} - \cos\gamma_{1,2}\right) \pm \frac{2\lambda}{3}, \tag{13}$$

where

$$\gamma_1 = \begin{cases} \frac{1}{3}\arctan\left(\frac{12\sqrt{3}|M_0|\xi_1}{\xi_2}\right) + \frac{\pi}{3}, & \xi_2 < 0 \\ \frac{1}{3}\arctan\left(\frac{12\sqrt{3}|M_0|\xi_1}{\xi_2}\right), & \xi_2 > 0, \end{cases} \tag{14}$$

$$\gamma_2 = \begin{cases} \frac{1}{3}\arctan\left(\frac{3\sqrt{3}|M_0|\xi_1}{-\xi_2}\right), & \xi_2 < 0 \\ \frac{1}{3}\arctan\left(\frac{3\sqrt{3}|M_0|\xi_1}{-\xi_2}\right) + \frac{\pi}{3}, & \xi_2 > 0, \end{cases} \tag{15}$$

with $\xi_1 = \sqrt{4{M_0}^4 + 13{M_0}^2\lambda^2 + 32\lambda^4}$ and $\xi_2 = -36{M_0}^2\lambda + 64\lambda^3$.

The localized states described by Eq. (13) exist inside the energy gap. This is shown explicitly in Fig. 2(a) where the

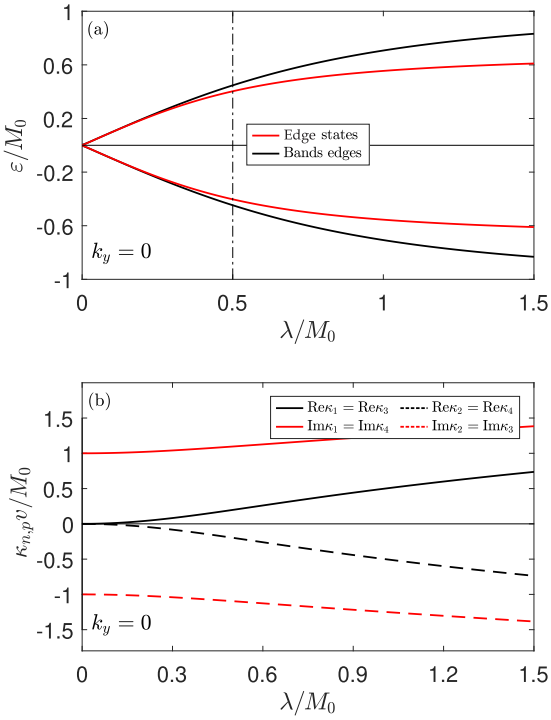

FIG. 2. (a) Energy of the electron states (for $k_y = 0$) localized at the domain wall (red lines) as a function of λ for $M_0 = 20$ meV. Black lines correspond to the edges of the gap in the bulk spectrum. Both, the energy ϵ and Rashba parameter λ are normalized to M_0. The vertical dashed-dot line marks the value of λ/M_0 used in the following figures. (b) Real and imaginary parts of $\kappa_{n,p}$ (normalized to M_0/v) defined by Eqs. (8) and (9) for $k_y = 0$.

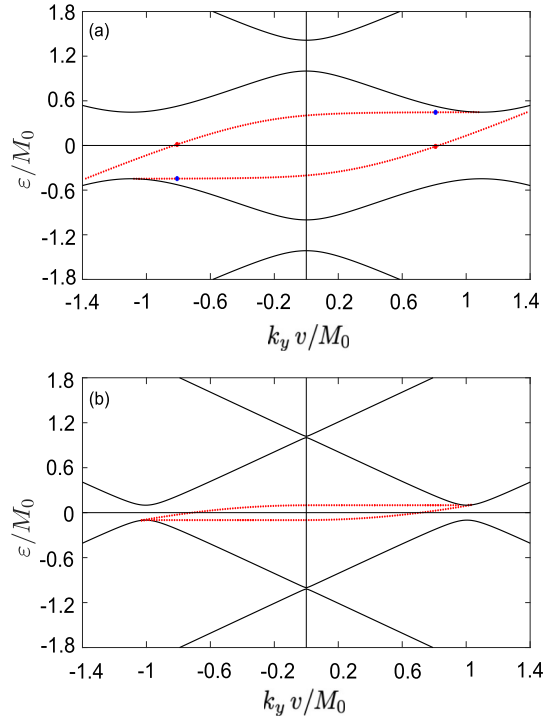

FIG. 3. Edge modes (red dotted lines) localized at the domain wall, presented as a function of k_y (normalized to M_0/v) for (a) $\lambda/M_0 = 0.5$, $\lambda = 10$ meV and (b) $\lambda/M_0 = 0.1$, $\lambda = 2$ meV. In both plots $M_0 = 20$ meV. The solid black lines determine the relevant conduction and valance bulk bands of graphene with Rashba spin-orbit coupling and magnetization. The large red and blue dots on the dispersion curves of the edge states correspond to the modes chosen in Figs. 4 and 5. The two red points (as well as the blue ones) are related by symmetry. Dispersion curves of the edge modes in the K and K' points are the same.

two energy levels $\varepsilon_{1,2}$ are presented by the red lines as a function of the spin-orbit coupling constant λ normalized to M_0. We remind one that these energy levels correspond to $k_y = 0$. The black lines in this figure describe the valence and conduction band edges (and thus determine the energy gap). The corresponding real and imaginary parts of the parameters $\kappa_{n,p}$ (normalized to M_0/v) are shown in Fig. 2(b). This figure clearly shows that $\kappa_{1,3}$ have positive real parts, and thus describe exponential localization of the wave function on the left side ($x < 0$), while the real parts of $\kappa_{2,4}$ are negative and describe exponential localization at the domain wall on the right side of the wall ($x > 0$). All the parameters κ also have imaginary parts.

IV. DISPERSION CURVES OF THE EDGE STATES

Now we determine the modes localized at the domain wall for nonzero values of k_y. All the calculation steps for $k_y \neq 0$ are similar to those for $k_y = 0$, but the derived formulas are cumbersome so they will not be presented here. Instead, we will show some numerical results. Energy $\varepsilon_{1(2)}$ of the lower (higher) edge mode is presented in Fig. 3(a) as a function of k_y normalized to M_0/v [$k_y/(M_0/v) = k_y v/M_0$] and for $\lambda/M_0 = 0.5$. These modes occur in the energy gap, but when they enter the conduction or valence bands, they acquire quasilocalized (or resonant) character due to interaction with the bulk electron bands. From symmetry (see Appendix A) follows that the whole spectrum is antisymmetric. This is clearly seen in Fig. 3(a), where $\varepsilon_1(k_y) = -\varepsilon_2(-k_y)$.

When the Rashba parameter λ decreases, the two localized modes in each Dirac point close up, as shown in Fig. 3(b) for a small value of the parameter λ. When λ tends to zero, these modes become degenerate and their energy tends to zero. In addition, they acquire the bulk character in the limit $\lambda \to 0$ since the inverse localization length $\mathrm{Re}\,\kappa$ tends then to zero [see also Fig. 2(b)].

Due to the imaginary terms in $\kappa_{n,p}$, the wave functions have a nonzero oscillatory contribution, as clearly visible in Fig. 4, where the probability density $p = \psi^\dagger(x)\psi(x)$ (normalized to M_0/v) is shown as a function of the dimensionless parameter xM_0/v (position on the axis x perpendicular to the wall, normalized to v/M_0) for the modes indicated by the red and blue dots on the dispersion curves of the edge modes in Fig. 3(a) for the point K. This probability density decays on both sides with the distance from the domain wall. However, this decay has exponential and oscillatory contributions. Amplitude of the oscillatory term decreases with increasing distance from the domain wall as well. As a result, expected values of some physical quantities in the edge states may behave in a similar manner. The period of the spatial oscillations is determined by the imaginary part of κ in Eqs. (8) and (9). For small $\epsilon < \lambda$

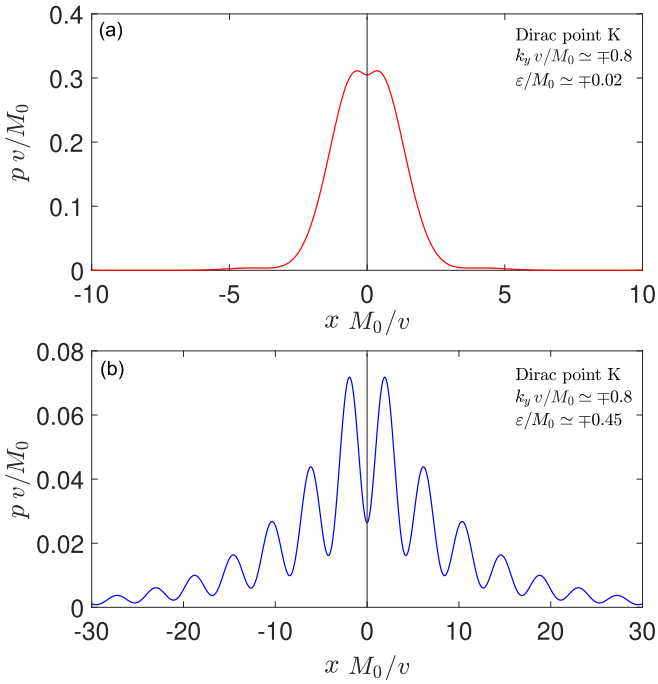

FIG. 4. (a) Normalized probability density p as a function of x for the edge states corresponding to the red (a) and blue (b) points on the dispersion curves in Fig. 3(a), and described by the energy ε/M and normalized wave vector k_y as indicated. Due to symmetry relations, these curves describe the probability density for the K and K' Dirac points. Other parameters: $\lambda/M = 0.5$ and $M_0 = 20$ meV.

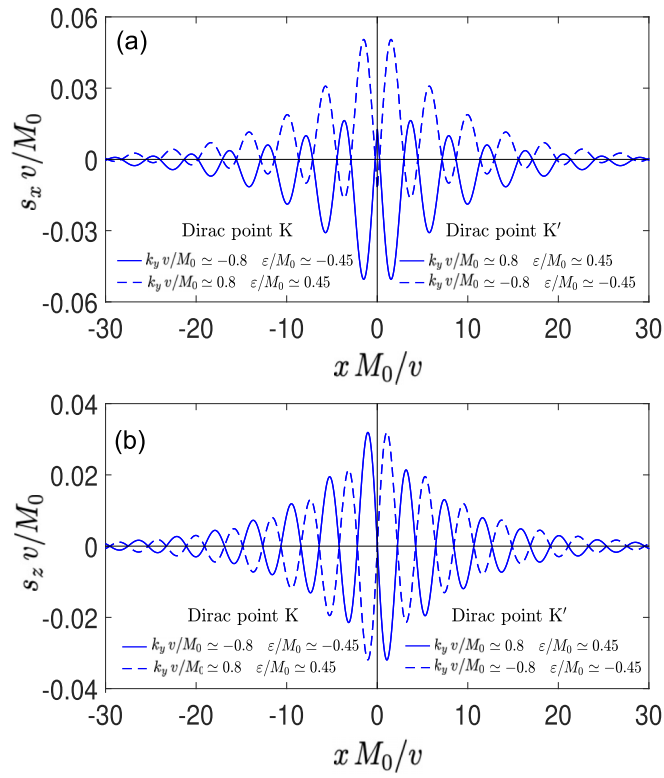

FIG. 5. Normalized spin density s_x (a) and s_z (b) for the Dirac points K and K'. The assumed parameters as indicated (they correspond to the blue points in Fig. 3). Other parameters: $\lambda/M = 0.5$ and $M_0 = 20$ meV.

and small λ we get a period $\sim v/M_0$. It is evident that the wave functions become more extended and the oscillations are more pronounced when the energy of the edge modes approaches one of the two gap edges.

We emphasize that all the results presented up to now correspond to the Dirac point K in the Brillouin zone. Similar modes exist also in the second Dirac point, K'. The corresponding Hamiltonian for the K' point reads

$$\hat{H}_{K'} = -iv\,(\tau_x\partial_x - \tau_y\partial_y) + \lambda(\sigma_y\tau_x + \sigma_x\tau_y) + \sigma_z M(x). \quad (16)$$

Calculations similar to those described above for the point K show that the edge modes (localized at the domain wall) associated with the point K' are exactly the same as the modes corresponding to the point K. Accordingly, the results shown in Figs. 2, 3, and 4 apply also to the point K'.

V. SPIN DENSITY ASSOCIATED WITH THE CHIRAL STATES

Now we consider spatial variation of the spin density associated with individual edge states, $\mathbf{s}(x) = \psi^\dagger(x)\tau_0\boldsymbol{\sigma}\psi(x)$, where τ_0 is the unit matrix in the sublattice space of graphene. In Fig. 5(a) we show the x component of the spin density, s_x, normalized to M_0/v as a function of xM_0/v for the modes indicated by the blue points in Fig. 3(a) for the K and K' points. Note, the x components of the spin density in these two symmetry-related points oscillates with increasing distance from the wall with opposite phases. Consequently, when both modes are populated, their contributions cancel each other. Apart from this, s_x is a symmetric function of x. Qualitatively similar behavior can be observed for the z components of the spin density, s_z. However, now the corresponding x dependence is antisymmetric. In turn, the y component of the spin density vanishes exactly, $s_y(x) = 0$.

From Fig. 5 follows that (i) the local spin density is oriented in the (x, z) plane and (ii) its magnitude decays in an oscillatory manner with increasing distance from the domain wall. The oscillation period depends on the wave vector, as shown in Fig. 6, where the local density of s_x and s_z (normalized to M_0/v) is shown for both edge modes as a function of the normalized wave vector and position on the axis x.

Here, it is interesting to note some similarity to the problem of *orthogonal spin polarization* at the Rashba-field domain wall in a homogeneously magnetized nanowire [42]. Even though the Hamiltonian of graphene differs substantially from the one-dimensional Rashba model considered in Ref. [42], a nonzero s_x at the graphene domain wall corresponds to orthogonal spin polarization since the x axis in our model is orthogonal to M and to the Rashba field when we consider electrons moving along the axis x (like in the nanowire problem).

Let us analyze now the total expected spin components S_x and S_z in the individual edge states considered above, i.e., the corresponding spin density integrated over x, $S_x = \int dx\, s_x(x)$ and $S_z = \int dx\, s_z(x)$. From the above analysis follows that S_x

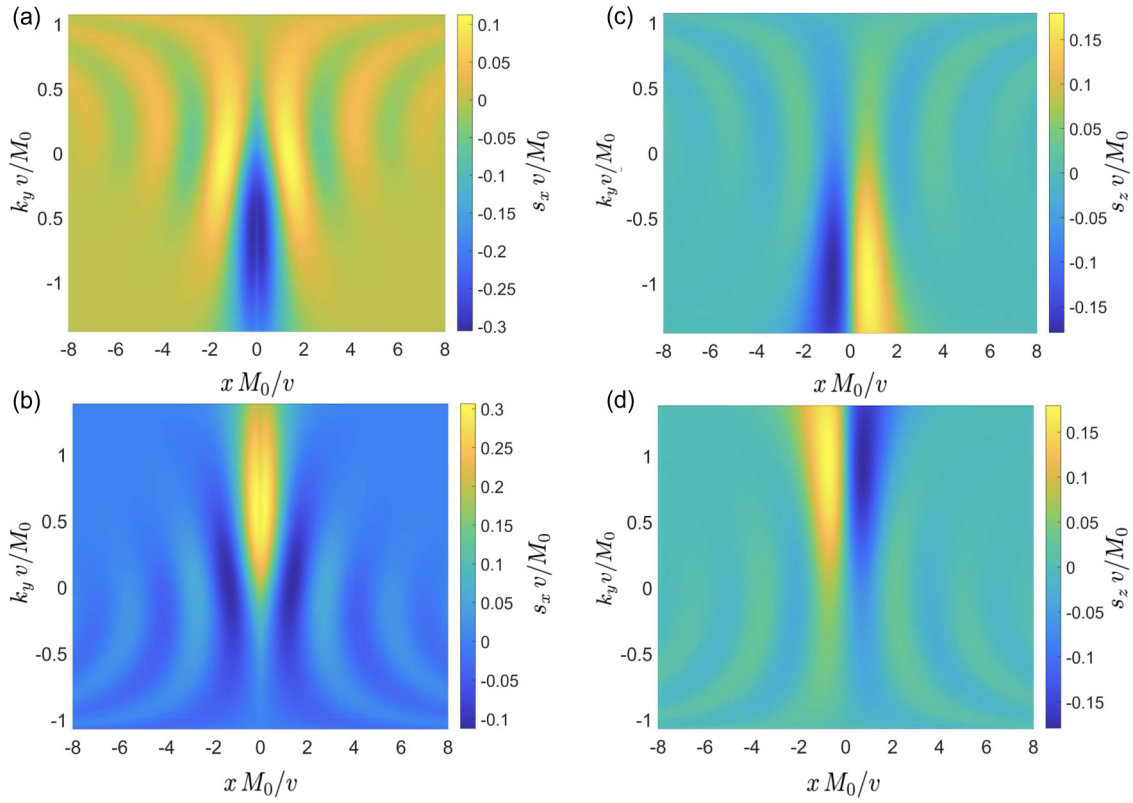

FIG. 6. The x and z components of spin density associated with the edge modes of higher (a),(c) and lower (b),(d) energy, presented as a function of the corresponding normalized wave vector k_y and normalized position x on the axis normal to the domain wall.

in a particular chiral state is generally nonzero, while the S_z component vanishes for all edge states. Therefore, we will focus now only on the S_x component. For a particular energy there are two edge states in the gap. For each Dirac point we define the total spin $S_x^t(\varepsilon)$ associated with edge modes at this energy as a sum of the contributions from the two states. In Fig. 7 we show S_x^t as a function of energy. The total spin polarization of the edge states is opposite for the points K and K'. Thus, the integrated spin polarization, obtained by integration over energy up to the Fermi level, vanishes due to compensation of the contributions from both Dirac points. To get a nonzero value of the integrated polarization one needs to lift the valley degeneracy.

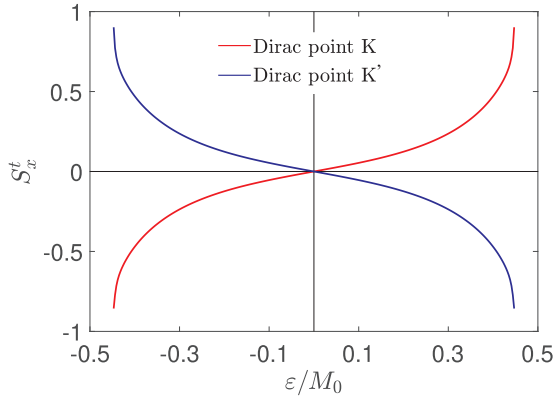

FIG. 7. Total spin S_x^t associated with the edge states in the K and K' points, presented as a function of energy for $\lambda/M = 0.5$.

VI. BULK-EDGE CORRESPONDENCE AND QUANTUM ANOMALOUS HALL EFFECT

The effective Hamiltonian describing bulk states on the right/left part of the system, i.e., of a single magnetic domain, is given by the extended Kane-Mele model [39],

$$\hat{H}_{K,K'} = v(\tau_x k_x + \eta_z \tau_y k_y) + \lambda(\eta_z \sigma_x \tau_y + \sigma_y \tau_x) + \sigma_z M, \quad (17)$$

where we introduced the Pauli matrix η_z acting in the valley subspace. Adding interaction with the perpendicular magnetization to the Hamiltonian of a pristine graphene leads to splitting of the energy bands, as presented in Fig. 1(c). In this case spin is still a good quantum number. The accidental crossing at two points with zero energy can be easily removed by a spin-mixing term, that is, by the Rashba spin-orbit interaction in our case. In turn, simultaneous action of magnetization and Rashba field opens an energy gap in the bulk spectrum [see Figs. 1(e) and 1(f)]. Thus, the perpendicular to plane magnetization breaks the time-reversal symmetry, while the Rashba coupling is a consequence of the inversion symmetry breaking and leads to the mixing of spin states. The insulating state, which appears when the energy gap is open, is topologically nontrivial and is called the quantum anomalous Hall (QAH) phase [43–45]. Accordingly, when the Fermi energy is in the energy gap, one may expect the QAH conductance of the system. Based on the Thouless-Kohmoto-Nightingale-Nijs) theory [46,47], the conductance is then given by the following simple expression:

$$\sigma_{xy} = \frac{e^2}{h} n_{Ch}, \quad (18)$$

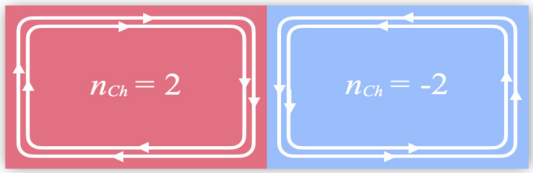

FIG. 8. Schematic picture of the bulk-edge correspondence for the structure presented in Fig. 1(a). The graphene domains with opposite magnetizations possess opposite Chern numbers. Accordingly, the two domains possess counterpropagating chiral edge states.

where

$$n_{Ch} = \frac{1}{2\pi} \sum_{\nu} \sum_{n} \int d^2\mathbf{k}\, \Omega^{\nu}_{z,n}(\mathbf{k}) \equiv n^{K}_{Ch} + n^{K'}_{Ch} \tag{19}$$

is the Chern number, and $\Omega^{\nu}_{z,n}(\mathbf{k})$ is the z component of the Berry curvature for the nth band in the momentum space (ν indicates one of the two inequivalent K points in graphene), whereas the summation over n is the summation over all occupied bands. For the effective continuum model [Eq. (17)] describing bulk states in the system with a single magnetic domain we find $n_{Ch} = 2\,\mathrm{sgn}(M)$, with the same contributions from the K and K' points, i.e., $n^{K}_{Ch} = n^{K'}_{Ch} = 1\,\mathrm{sgn}(M)$ [41,48–50]. According to the bulk-boundary correspondence, one can then expect two chiral edge modes (see Fig. 8), at the interface between graphene and vacuum, that is between two topologically distinct phases, i.e., between the QAH phase and the trivial insulator.

The system with a magnetization kink (sharp domain wall) can be considered as a junction of two QAH insulators with opposite chiralities of the edge modes (the orientation of magnetization determines the sign of the Berry curvature) that have been connected adiabatically. This is reminiscent of the generalized Jackiw-Rebbi model for Dirac fermions in graphene with the magnetization kink, $M(x) = -M(-x)$. Accordingly, we have a pair of topologically different topological insulators [$n_{Ch}(x < 0) = 2$ and $n_{Ch}(x > 0) = -2$], which belong to the same symmetry class [51]. Thus, one can expect four edge states propagating in the same direction along the domain wall, as presented in Fig. 8. The quantized anomalous Hall conductivity at the domain wall is equal to $-4e^2/h$.

However, it should be stressed that the edge states at the magnetization kink are not protected against scattering as the interface is not between topologically distinct insulators [51,52]. More precisely, there are two topologically distinct regions (phases) defined by different Chern numbers, but Hamiltonians describing these regions belong to the same class of topological order. Secondly, for graphene one cannot limit backward-scattering processes to energy states around a single Dirac cone (single valley). Note that the time-reversal symmetry for graphene is defined by the operator $\Theta = i\eta_x\sigma_y\mathcal{K}$ [53] where $\mathcal{K}$ is a complex conjugation. Due to the last term in the Hamiltonian (17) the time-reversal symmetry is broken, i.e., $\Theta H(\mathbf{k})\Theta^{-1} \neq H(-\mathbf{k})$. Consequently, the intervalley scattering processes are allowed. In Appendix A we provide a more detailed discussion of the symmetry of the system under consideration.

The problem of intervalley scattering is an important issue in the context of the realization of QAH effect in real graphene–based systems. It should be mentioned that the realization of graphene in the presence of the net perpendicular to plain magnetization and Rashba spin-orbit coupling is possible in several ways. One of the reported methods relies on the absorption of magnetic transition-metal adatoms on one side of the graphene layer. This ensures not only magnetic proximity effect, but also a charge transfer between graphene and adatoms, which leads to a sizable Rashba effect [54–58]. This solution is, however, related to the intervalley scattering and diminishing of the QAH phase. Jiang *et al.* [59] showed that the QAH phase can survive when the magnetic adatoms are distributed in a completely random way. Such a solution is rather difficult to achieve in realistic samples, as adatoms in graphene prefer to form clusters that destroy the QAH phase [60,61]. Another realization is based on the deposition of graphene on a ferromagnetic insulating substrate like yttrium iron garnet, $RbMnCl_3$, or $LaMnO_3$ [62–64]. However, the Rashba spin-orbit coupling in such systems is weak and thus the energy gap is also rather small.

VII. SUMMARY AND CONCLUSIONS

We have considered the energy spectrum of a system consisting of a graphene monolayer with spin-orbit Rashba interaction, which is additionally coupled to a magnetic layer with a domain wall. The main focus was on the states localized at the domain wall, which exist in the gap created by coupling to the ferromagnetic layer in the presence of Rashba spin-orbit interaction. For each Dirac point we found two one-dimensional bands of chiral modes, and the modes in different points are similar. We have also calculated expected values of the spin density as well as the total spin expected in the edge states. We have shown that the spin polarization of the edge states appears when there is an imbalance in the occupations of the K and K' Dirac points.

From symmetry follows that $\varepsilon^{K}(k_y) = -\varepsilon^{K}(-k_y)$ (the same for the K' point), and also $\varepsilon^{K}(k_y) = \varepsilon^{K'}(k_y)$. Different domains correspond to topologically different regions defined by different Chern numbers (2 and -2 on different sides of the wall). From this analysis follows that four chiral states propagate along the domain wall when the Fermi energy is in the gap, exactly what was found from direct calculations of the modes localized at the wall. As a consequence, one can observe quantized anomalous Hall conductance along the domain wall with four conductance quanta. However, the chiral states at the domain wall are not protected against intervalley scattering. Such scattering processes can lead to a suppression of QAH effect. More details on scattering are given in Appendix B.

In our considerations we assumed a domain wall with equal magnitudes $|M| = M_0$ of magnetization on both sides. When M on one side of the wall is small, the corresponding gap is narrow, and one can expect that two chiral modes at the wall are low energy and slowly decay with distance from the wall. Obviously, when $M = 0$ on one side, the second part of the system is then covered by a uniform magnetic domain and it is in the QAH phase, while the part with $M = 0$ is in the metallic phase.

ACKNOWLEDGMENTS

This work was partially supported by the National Science Centre in Poland under the Project No. DEC-2017/27/B/ST3/02881 (M.I., V.K., and J.B.) and by the Norwegian Financial Mechanism under the Polish-Norwegian Research Project NCN GRIEG "2Dtronics," Project No. 2019/34/H/ST3/00515 (A.D.).

APPENDIX A: SYMMETRY OF THE SYSTEM

Time-inversion operator for $\hat{H}(k_y)$ is $T_t = \tau_y\sigma_y\mathcal{K}\mathcal{P}_{k_y}$, where $\mathcal{K}$ stands for the complex conjugation and $\mathcal{P}_{k_y}$ changes $k_y \to -k_y$. The Hamiltonian $\hat{H}_0$ is invariant with respect to this transformation, $T_t\hat{H}_0T_t^\dagger = \hat{H}_0$. The term $\sigma_z M$ in $\hat{H}$ breaks this symmetry, but reversing simultaneously the sign of M leads to $T_t\,\hat{H}(M)\,T_t^\dagger = \hat{H}(-M)$.

One can introduce electron-hole inversion operator $T_c = \tau_y\sigma_x\mathcal{K}$. If M is constant, we consider $\hat{H}_{K,K'}(\mathbf{k}) = v(\tau_x k_x \pm \tau_y k_y) + \lambda(\mp\sigma_x\tau_y + \sigma_y\tau_x) + \sigma_z M$. In this case $T_c\,\hat{H}(\mathbf{k})\,T_c^\dagger = -\hat{H}(\mathbf{k})$, which means that if $\psi_{\mathbf{k}}$ is the eigenfunction of $\hat{H}(\mathbf{k})$ with the eigenvalue $\varepsilon(\mathbf{k})$, then $T_c\psi_{\mathbf{k}}$ is also the eigenfunction of $\hat{H}(\mathbf{k})$ with the eigenvalue $-\varepsilon(\mathbf{k})$. This corresponds to electron-hole symmetry for $\hat{H}(\mathbf{k})$. When M is not constant, e.g., for $M(x) = -M(-x)$, this symmetry is broken.

Let us consider now the transformation $T_p = \tau_x$, for which we get $T_p\,\hat{H}_K(k_y)\,T_p^\dagger = \hat{H}_{K'}(k_y)$. This indicates that if $\psi_{k_y}(x)$ is the eigenfunction of $\hat{H}_K$ with the eigenvalue $\varepsilon(k_y)$, then the function $T_p\,\psi_{k_y}(x)$ is also the eigenfunction of $\hat{H}_{K'}$ with the same eigenvalue $\varepsilon(k_y)$.

There is one more transformation $T_r = \sigma_z\mathcal{P}_x\mathcal{P}_{k_y}$, which acts as $T_r\,\hat{H}_{K,K'}(k_y)T_r^\dagger = -\hat{H}_{K,K'}(-k_y)$ when $M(x) = -M(-x)$ (this is the symmetry of our model). It leads to $\varepsilon(k_y) = -\varepsilon(-k_y)$. Thus, the dependence $\varepsilon(k_y)$ is an antisymmetric function of k_y.

Let us introduce vector $\mathbf{R} = \mathbf{m}(-\delta) \times \mathbf{m}(+\delta)$, where $\mathbf{m}(x) = \mathbf{M}(x)/M_0$. This vector determines the chirality. As one can conclude from Fig. 3, the group velocity of electrons localized at the domain wall is in the direction of $\mathbf{R}$ for both valleys K and K'.

APPENDIX B: BACKWARD SCATTERING FROM IMPURITIES

From the above symmetry considerations follows that for each Dirac point the T_r symmetry relates the states k_y and $-k_y$ with opposite signs of energy. Therefore, such a symmetry does not impose any restrictions on elastic scattering from defects as long as there is only one state with certain value of $k_y = k_{y0}$, for which $\varepsilon(k_{y0}) = \varepsilon(-k_{y0}) = 0$. In principle, the T_r symmetry in this case could be important if the perturbation does not break this symmetry. However, considering the scattering matrix $\hat{S}$, which relates scattering states in different channels for the case of functions ψ and $T_r\psi$, we found that T_r does not impose any additional restrictions to the scattering matrix. One should also note that the usual impurity with potential $V(\mathbf{r})$ located at some point in the domain wall breaks explicitly the symmetry T_r because the impurity potential is even with respect to $x \to -x$. Correspondingly, such a symmetry cannot protect the edge states against scattering between $\mathbf{k}$ and $-\mathbf{k}$. Note that this is not a backward scattering since the electron velocity has the same sign for these states.

A mechanism which can lead to the absence of intravalley backward scattering is related to the peculiarity of electron band structure. Let us consider the wave functions of electrons in the edge states $|k_y\rangle = e^{ik_y y}\psi_{k_y}(x)$ and $|k'_y\rangle = e^{ik'_y y}\psi_{k'_y}(x)$ corresponding to energy ε in the gap. These states belong to different bands in the same valley (see Fig. 3). Matrix element $\langle k_y|V(\mathbf{r})|k'_y\rangle$ of the impurity perturbation located at the point $\mathbf{R} = 0$ (at the domain wall) is

$$\langle k_y|V(\mathbf{r})|k'_y\rangle = \int \frac{dq_x}{2\pi}\,V(q_x, k_y - k'_y) \times \int_{-\infty}^{\infty} dx\, e^{iq_x x}\psi^\dagger_{k_y}(x)\,\psi_{k'_y}(x), \qquad \text{(B1)}$$

where $V(q_x, q_y)$ is the Fourier transform of the impurity potential. We calculated the wave functions $\psi_{k_y}(x)$ and $\psi_{k'_y}(x)$ numerically, and using these results we found that $\psi_{k_y}(x)$ and $\psi_{k'_y}(x)$ are numerically orthogonal (the integral of nonorthogonality was negligible for the normalized wave functions). From this we conclude that the probability of impurity scattering from k_y to k'_y is negligible.

[1] M. Z. Hasan and C. L. Kane, *Colloquium*: Topological insulators, Rev. Mod. Phys. **82**, 3045 (2010).

[2] X.-L. Qi and S.-C. Zhang, Topological insulators and superconductors, Rev. Mod. Phys. **83**, 1057 (2011).

[3] H. Zhang, C.-X. Liu, X.-L. Qi, X. Dai, Z. Fang, and S.-C. Zhang, Topological insulators in Bi_2Se_3, Bi_2Te_3 and Sb_2Te_3 with a single Dirac cone on the surface, Nat. Phys. **5**, 438 (2009).

[4] L. Fu, Topological Crystalline Insulators, Phys. Rev. Lett. **106**, 106802 (2011).

[5] Y. Ando and L. Fu, Topological crystalline insulators and topological superconductors: From concepts to materials, Annu. Rev. Condens. Matter Phys. **6**, 361 (2015).

[6] Q. Liu, C.-X. Liu, C. Xu, X.-L. Qi, and S.-C. Zhang, Magnetic Impurities on the Surface of a Topological Insulator, Phys. Rev. Lett. **102**, 156603 (2009).

[7] Y. L. Chen, J.-H. Chu, J. G. Analytis, Z. K. Liu, K. Igarashi, H.-H. Kuo, X. L. Qi, S. K. Mo, R. G. Moore, D. H. Lu, M. Hashimoto, T. Sasagawa, S. C. Zhang, I. R. Fisher, Z. Hussain, and Z. X. Shen, Massive Dirac fermion on the surface of a magnetically doped topological insulator, Science **329**, 659 (2010).

[8] Y. Ferreiros, F. J. Buijnsters, and M. I. Katsnelson, Dirac electrons and domain walls: A realization in junctions of ferromagnets and topological insulators, Phys. Rev. B **92**, 085416 (2015).

[9] K. Yasuda, M. Mogi, R. Yoshimi, A. Tsukazaki, K. S. Takahashi, M. Kawasaki, F. Kagawa, and Y. Tokura, Quantized chiral edge conduction on domain walls of a magnetic topological insulator, Science **358**, 1311 (2017).

[10] M. Sedlmayr, N. Sedlmayr, J. Barnaś, and V. K. Dugaev, Chiral Hall effect in the kink states in topological insulators with magnetic domain walls, Phys. Rev. B **101**, 155420 (2020).

[11] Y. Araki, A. Yoshida, and K. Nomura, Universal charge and current on magnetic domain walls in Weyl semimetals, Phys. Rev. B **94**, 115312 (2016).

[12] R. Jackiw and C. Rebbi, Solitons with fermion number 1/2, Phys. Rev. D **13**, 3398 (1976).

[13] B. A. Volkov and O. A. Pankratov, Heavy fermions in a supersymmetric ferroelectric domain wall, J. Exp. Theor. Phys. Lett. **43**, 130 (1986).

[14] G. E. Volovik, Fermion zero modes on vortices in chiral superconductors, J. Exp. Theor. Phys. Lett. **70**, 609 (1999).

[15] Y. Nishida, L. Santos, and C. Chamon, Topological superconductors as nonrelativistic limits of Jackiw-Rossi and Jackiw-Rebbi models, Phys. Rev. B **82**, 144513 (2010).

[16] D.-H. Lee, G.-M. Zhang, and T. Xiang, Edge Solitons of Topological Insulators and Fractionalized Quasiparticles in Two Dimensions, Phys. Rev. Lett. **99**, 196805 (2007).

[17] D. Bercioux and A. De Martino, Spin-orbit interaction and snake states in a graphene *p-n* junction, Phys. Rev. B **100**, 115407 (2019).

[18] F. Ronetti, K. Plekhanov, D. Loss, and J. Klinovaja, Magnetically confined bound states in Rashba systems, Phys. Rev. Research **2**, 022052(R) (2020).

[19] F. Dolcini and F. Rossi, Magnetic field effects on a nanowire with inhomogeneous Rashba spin-orbit coupling: Spin properties at equilibrium, Phys. Rev. B **98**, 045436 (2018).

[20] Y. S. Gani, E. J. Walter, and E. Rossi, Proximity-induced spin-orbit splitting in graphene nanoribbons on transition-metal dichalcogenides, Phys. Rev. B **101**, 195416 (2020).

[21] F. Dolcini, Interplay between Rashba interaction and electromagnetic field in the edge states of a two-dimensional topological insulator, Phys. Rev. B **95**, 085434 (2017).

[22] L. Ju, Z. Shi, N. Nair, Y. Lv, C. Jin, J. Velasco, Jr., C. Ojeda-Aristizabal, H. A. Bechtel, M. C. Martin, A. Zettl, J. Analytis, and F. Wang, Topological valley transport at bilayer graphene domain walls, Nature (London) **520**, 650 (2015).

[23] F. Escudero, L. Sourrouille, J. S. Ardenghi, and P. Jasen, Magnetization in pristine graphene with Zeeman splitting and variable spin-orbit coupling, Superlattices Microstruct. **101**, 537 (2017).

[24] T. Ono, H. Miyajima, K. Shigeto, K. Mibu, N. Hosoito, and T. Shinjo, Propagation of a magnetic domain wall in a submicrometer magnetic wire, Science **284**, 468 (1999).

[25] J. Trützschler, K. Sentosun, B. Mozooni, R. Mattheis, and J. McCord, Magnetic domain wall gratings for magnetization reversal tuning and confined dynamic mode localization, Sci. Rep. **6**, 30761 (2016).

[26] S. S. P. Parkin, M. Hayashi, and L. Thomas, Magnetic domain-wall racetrack memory, Science **320**, 190 (2008).

[27] E. Saitoh, H. Miyajima, T. Yamaoka, and G. Tatara, Current-induced resonance and mass determination of a single magnetic domain wall, Nature (London) **432**, 203 (2004).

[28] D. A. Allwood, G. Xiong, C. C. Faulkner, D. Atkinson, D. Petit, and R. P. Cowburn, Magnetic domain-wall logic, Science **309**, 1688 (2005).

[29] M. Hayashi, L. Thomas, R. Moriya, C. Rettner, and S. S. P. Parkin, Current-controlled magnetic domain-wall nanowire shift register, Science **320**, 209 (2008).

[30] P. Krzysteczko, J. Wells, A. Fernández Scarioni, Z. Soban, T. Janda, X. Hu, V. Saidl, R. P. Campion, R. Mansell, J.-H. Lee, R. P. Cowburn, P. Nemec, O. Kazakova, J. Wunderlich, and H. W. Schumacher, Nanoscale thermoelectrical detection of magnetic domain wall propagation, Phys. Rev. B **95**, 220410(R) (2017).

[31] C. Lee, G. Kim, J. Jung, and H. Min, Zero-line modes at stacking faulted domain walls in multilayer graphene, Phys. Rev. B **94**, 125438 (2016).

[32] G. W. Semenoff, V. Semenoff, and F. Zhou, Domain Walls in Gapped Graphene, Phys. Rev. Lett. **101**, 087204 (2008).

[33] Z. Wang, D.-K. Ki, J. Y. Khoo, D. Mauro, H. Berger, L. S. Levitov, and A. F. Morpurgo, Origin and Magnitude of Designer Spin-Orbit Interaction in Graphene on Semiconducting Transition Metal Dichalcogenides, Phys. Rev. X **6**, 041020 (2016).

[34] T. Frank, M. Gmitra, and J. Fabian, Theory of electronic and spin-orbit proximity effects in graphene on Cu(111), Phys. Rev. B **93**, 155142 (2016).

[35] H.-Y. Yang, C. Huang, H. Ochoa, and M. A. Cazalilla, Extrinsic spin Hall effect from anisotropic Rashba spin-orbit coupling in graphene, Phys. Rev. B **93**, 085418 (2016).

[36] I. I. Klimovskikh, O. Vilkov, D. Y. Usachov, A. G. Rybkin, S. S. Tsirkin, M. V. Filianina, K. Bokai, E. V. Chulkov, and A. M. Shikin, Variation of the character of spin-orbit interaction by Pt intercalation underneath graphene on Ir(111), Phys. Rev. B **92**, 165402 (2015).

[37] P. Leicht, J. Tesch, S. Bouvron, F. Blumenschein, P. Erler, L. Gragnaniello, and M. Fonin, Rashba splitting of graphene-covered Au(111) revealed by quasiparticle interference mapping, Phys. Rev. B **90**, 241406(R) (2014).

[38] M. Khodas, I. A. Zaliznyak, and D. E. Kharzeev, Spin-polarized transport through a domain wall in magnetized graphene, Phys. Rev. B **80**, 125428 (2009).

[39] C. L. Kane and E. J. Mele, Quantum Spin Hall Effect in Graphene, Phys. Rev. Lett. **95**, 226801 (2005).

[40] L. Frąckowiak, P. Kuświk, G. D. Chaves-O'Flynn, M. Urbaniak, M. Matczak, P. P. Michałowski, A. Maziewski, M. Reginka, A. Ehresmann, and F. Stobiecki, Magnetic Domains without Domain Walls: A Unique Effect of He^+ ion Bombardment in Ferrimagnetic Tb/Co films, Phys. Rev. Lett. **124**, 047203 (2020).

[41] A. Dyrdał and J. Barnaś, Anomalous, spin, and valley Hall effects in graphene deposited on ferromagnetic substrates, 2D Mater. **4**, 034003 (2017).

[42] L. Rossi, F. Dolcini, and F. Rossi, Majorana-like localized spin density without bound states in topologically trivial spin-orbit coupled nanowires, Phys. Rev. B **101**, 195421 (2020).

[43] F. D. M. Haldane, Model for a Quantum Hall Effect without Landau Levels: Condensed-Matter Realization of the Parity Anomaly, Phys. Rev. Lett. **61**, 2015 (1988).

[44] H. Weng, R. Yu, X. Hu, X. Dai, and Z. Fang, Quantum anomalous Hall effect and related topological electronic states, Adv. Phys. **64**, 227 (2015).

[45] Y. Ren, Z. Qiao, and Q. Niu, Topological phases in two-dimensional materials: A review, Rep. Prog. Phys. **79**, 066501 (2016).

[46] D. J. Thouless, M. Kohmoto, M. P. Nightingale, and M. den Nijs, Quantized Hall Conductance in a Two-Dimensional Periodic Potential, Phys. Rev. Lett. **49**, 405 (1982).

[47] Q. Niu, D. J. Thouless, and Y.-S. Wu, Quantized Hall conductance as a topological invariant, Phys. Rev. B **31**, 3372 (1985).

[48] Z. Qiao, S. A. Yang, W. Feng, W.-K. Tse, J. Ding, Y. Yao, J. Wang, and Q. Niu, Quantum anomalous Hall effect in graphene from Rashba and exchange effects, Phys. Rev. B **82**, 161414(R) (2010).

[49] Z. Qiao, H. Jiang, X. Li, Y. Yao, and Q. Niu, Microscopic theory of quantum anomalous Hall effect in graphene, Phys. Rev. B **85**, 115439 (2012).

[50] P. Högl, T. Frank, K. Zollner, D. Kochan, M. Gmitra, and J. Fabian, Quantum Anomalous Hall Effects in Graphene from Proximity-Induced Uniform and Staggered Spin-Orbit and Exchange Coupling, Phys. Rev. Lett. **124**, 136403 (2020).

[51] C.-K. Chiu, J. C. Y. Teo, A. P. Schnyder, and S. Ryu, Classification of topological quantum matter with symmetries, Rev. Mod. Phys. **88**, 035005 (2016).

[52] J. Cayssol, Introduction to Dirac materials and topological insulators, C. R. Phys. **14**, 760 (2013).

[53] J. Inoue, A. Yamakage, and S. Honda, *Graphene in Spintronics: Fundamentals and Applications*, 1st ed. (Jenny Stanford Publishing, New York, 2016).

[54] J. Ding, Z. Qiao, W. Feng, Y. Yao, and Q. Niu, Engineering quantum anomalous/valley Hall states in graphene via metal-atom adsorption: An *ab initio* study, Phys. Rev. B **84**, 195444 (2011).

[55] H. Zhang, C. Lazo, S. Blügel, S. Heinze, and Y. Mokrousov, Electrically Tunable Quantum Anomalous Hall Effect in Graphene Decorated by 5*d* Transition-Metal Adatoms, Phys. Rev. Lett. **108**, 056802 (2012).

[56] Y. Dumeige, M. Chipaux, V. Jacques, F. Treussart, J.-F. Roch, T. Debuisschert, V. M. Acosta, A. Jarmola, K. Jensen, P. Kehayias, and D. Budker, Magnetometry with nitrogen-vacancy ensembles in diamond based on infrared absorption in a doubly resonant optical cavity, Phys. Rev. B **87**, 155202 (2013).

[57] Y. M. Lu, Y. Choi, C. M. Ortega, X. M. Cheng, J. W. Cai, S. Y. Huang, L. Sun, and C. L. Chien, Pt Magnetic Polarization on $\mathbf{Y}_3\mathrm{Fe}_5\mathbf{O}_{12}$ and Magnetotransport Characteristics, Phys. Rev. Lett. **110**, 147207 (2013).

[58] Y. Gong, A. G. Joly, D. Hu, P. Z. El-Khoury, and W. P. Hess, Ultrafast imaging of surface plasmons propagating on a gold surface, Nano Lett. **15**, 3472 (2015).

[59] H. Jiang, Z. Qiao, H. Liu, J. Shi, and Q. Niu, Stabilizing Topological Phases in Graphene via Random Adsorption, Phys. Rev. Lett. **109**, 116803 (2012).

[60] T. Eelbo, M. Waśniowska, P. Thakur, M. Gyamfi, B. Sachs, T. O. Wehling, S. Forti, U. Starke, C. Tieg, A. I. Lichtenstein, and R. Wiesendanger, Adatoms and Clusters of 3*d* Transition Metals on Graphene: Electronic and Magnetic Configurations, Phys. Rev. Lett. **110**, 136804 (2013).

[61] H. Chen, Q. Niu, Z. Zhang, and A. H. MacDonald, Gate-tunable exchange coupling between cobalt clusters on graphene, Phys. Rev. B **87**, 144410 (2013).

[62] Z. Qiao, W. Ren, H. Chen, L. Bellaiche, Z. Zhang, A. H. MacDonald, and Q. Niu, Quantum Anomalous Hall Effect in Graphene Proximity Coupled to an Antiferromagnetic Insulator, Phys. Rev. Lett. **112**, 116404 (2014).

[63] Z. Wang, C. Tang, R. Sachs, Y. Barlas, and J. Shi, Proximity-Induced Ferromagnetism in Graphene Revealed by the Anomalous Hall Effect, Phys. Rev. Lett. **114**, 016603 (2015).

[64] J. Zhang, B. Zhao, Y. Yao, and Z. Yang, Quantum anomalous Hall effect in graphene-based heterostructure, Sci. Rep. **5**, 10629 (2015).